

# ADVANCED MATERIALS

## Supporting Information

for *Adv. Mater.*, DOI: 10.1002/adma.201804089

A 3D Nitrogen-Doped Graphene/TiN Nanowires Composite  
as a Strong Polysulfide Anchor for Lithium–Sulfur Batteries  
with Enhanced Rate Performance and High Areal Capacity

*Zhaohuai Li, Qiu He, Xu Xu,\* Yan Zhao, Xiaowei Liu, Cheng  
Zhou, Dong Ai, Lixue Xia, and Liqiang Mai\**

## Supporting Information

### **Three-Dimensional Nitrogen-Doped Graphene/TiN Nanowire Composite as a Strong Polysulfide Anchor for Lithium-Sulfur Batteries with Enhanced Rate Performance and High Areal Capacity**

*Zhaohuai Li, Qiu He, Xu Xu,\* Yan Zhao, Xiaowei Liu, Cheng Zhou, Dong Ai, Lixue Xia and Liqiang Mai\**

#### **Experimental section**

**Preparation of a 3DNG/TiN composite.** The precursor  $\text{H}_2\text{Ti}_3\text{O}_7$  nanowires was synthesized according to a previous report.<sup>[1]</sup> Briefly,  $\text{TiO}_2$  anatase (1 g) was added into NaOH solution (30 mL, 15 M) under magnetic stirring to get homogeneous emulsion. Then, the suspension was transferred to a Teflon-lined stainless steel autoclave and stayed at 180 °C for 72 h. Then the product was stirred in 0.1 M HCl solution for 24 h and washed with deionized water and alcohol, finally, the  $\text{H}_2\text{Ti}_3\text{O}_7$  Nanowires were obtained after dried at 70 °C for 12 h. The GO was prepared through the typical Hummer method.<sup>[2]</sup> Afterwards, the GO and  $\text{H}_2\text{Ti}_3\text{O}_7$  Nanowires were mixed by ultrasound and stir, following by adding sodium ascorbate solution (1 M) and subsequent heat of the mixture at 95 °C for 2 h to fabricate 3DG/  $\text{H}_2\text{Ti}_3\text{O}_7$ . Finally, the obtained product was calcined at 800 °C for 2 h in  $\text{NH}_3$  (80 sccm) atmosphere. For comparison, 3DNG was prepared by the same procedure without adding TiN Nanowires. The 3DG/ $\text{TiO}_2$  composite was synthesized by heating 3DG/ $\text{H}_2\text{Ti}_3\text{O}_7$  at 600 °C in air.

**Preparation of the Li<sub>2</sub>S<sub>6</sub> electrolyte.** The Li<sub>2</sub>S<sub>6</sub> electrolyte was synthesized by reacting sulfur and Li<sub>2</sub>S at a molar ratio of 5:1, which added to precise configured liquid mixture of 1, 2-dimethoxyethane (DME) and 1, 3-dioxolane (DOL) (1:1 in volume) and homogenized by vigorous stirring at 70 °C for 48 hours.

**Adsorption test.** We adopted Li<sub>2</sub>S<sub>6</sub> as the representative of LiPSs to simplify the experiments and prepared the Li<sub>2</sub>S<sub>6</sub> solution with the concentration of 0.005 M. Before the LiPSs adsorption test, all the 3DNG, 3DG/TiO<sub>2</sub> and 3DNG/TiN of the same quantity were dried under vacuum at 70 °C for 12 h. After LiPSs adsorption test for the first time, the containers were sealed in a glove box filled with argon.

**Materials Characterization.** X-ray diffraction (XRD) characterization was performed to investigate the crystallographic information of samples using a D8 Advance X-ray diffractometer with a non-monochromated Cu Ka X-ray source ( $\lambda=1.054056 \text{ \AA}$ ). Scanning electron microscopy (SEM) images were collected by using a JEOL JSM- 7100F at an acceleration voltage of 15 kV. Transmission electron microscopy (TEM) and high resolution TEM (HRTEM) images were recorded with a Titan G2 60-300 with EDS image corrector. Brunauer–Emmett–Teller (BET) surface areas were measured using a Tristar II 3020 instrument by nitrogen adsorption at 77 K. Thermogravimetric analysis (TGA) was performed using a Netzsch STA 449C simultaneous analyzer. Raman spectra were obtained using a Renishaw in micro-Raman spectroscopy system. X-ray photoelectron spectroscopy (XPS) measurements were conducted using a VG MultiLab 2000 instrument.

**Electrical conductivity measurements.** The TiN and TiO<sub>2</sub> nanowires were first dispersed on the substrate. Metal contacts on single nanowire were patterned with e-beam lithography and deposition of Cr/Au (10/150 nm). The I–V test of single nanowire was carried out with a semiconductor device analyzer, with the devices electrically connected in the probe station. According to previous methods<sup>[3,4]</sup>, the electrical conductivities of 3DNG/TiN, 3DG/TiO<sub>2</sub> and 3DNG were measured by two-probe method.

**Electrochemical Measurement.** Stainless steel coin cells (2,025-type) were assembled in a glovebox filled with pure argon gas. A Celgard 2400 polypropylene membrane was used as the separator. The electrolyte was 1.0 M lithium bistrifluoromethanesulfonylimide dissolved in DOL (99.5%, Alfa Aesar) and DME (99.5%, Alfa Aesar) (1:1 ratio by volume) with 0.1 M lithium nitrate (LiNO<sub>3</sub>, 99.9%, Alfa Aesar) as the additive. The amount of Li<sub>2</sub>S<sub>6</sub> electrolyte in the cell was controlled to be 10 μL mg<sup>-1</sup> of sulfur. The Galvanostatic charge/discharge measurements were performed with a multichannel battery testing system (LAND CT2001A) in the potential range from 1.6-2.8 V at different current densities. Electrochemical impedance spectroscopy (EIS) tests (0.1 Hz-100 kHz, 5 mV) were conducted on an electrochemical workstation (Autolab PGSTAT302N). All the specific capacities were calculated based on the mass of active sulfur. The cycled cell was disassembled inside an Ar-filled glovebox to avoid oxidation, and the electrode was washed gently with DOL/DME solvent and dried inside the glove box at room temperature, then transferred with a sealed container and prepare for characterization.

**Theoretical Computation.** All the first-principles calculations have been performed within the density-functional theory (DFT) framework, as implemented in the Material Studio software. DMol<sup>3</sup><sup>15, 61</sup> and CASTEP<sup>[7]</sup> modules were adopted to calculate the adsorption energies of Li<sub>2</sub>S<sub>x</sub> ( $x=4, 6, 8$ ) and S<sub>8</sub> on the surfaces of the (200) plane of TiN, the (110) plane of TiO<sub>2</sub>, and N-doped reduced graphene oxide (NG). The heights of the vacuum slabs on the surfaces of these adsorbents are more than 10 Å in order to avoid the interactions between successive slabs. The thickness of the TiN (200) and TiO<sub>2</sub> (110) slabs is of 3 and 4 atom layers respectively. The *a* and *b* dimensions are 12.0038 × 12.0037 for the TiN (200) slab and 11.836 × 12.9938 Å for the TiO<sub>2</sub> (110) slab, as shown in periodic box. During the geometry optimization, the atoms in the TiN (200) and TiO<sub>2</sub> (110) slabs were fixed to their bulk truncated positions. All the geometry optimizations for the adsorption on the TiN (200) and TiO<sub>2</sub> (110) slabs have been preliminarily performed with the Dmol<sup>3</sup> module using a medium quality and then optimized with the CASTEP module. For the Dmol<sup>3</sup> calculations the energy displacement tolerance was 2.0 × 10<sup>-5</sup> Ha; the self-consistent field (SCF) tolerance was 1.0 × 10<sup>-5</sup> Ha;  $\Gamma$ -centered k-mesh was 1 × 1 × 1. For the CASTEP calculations, these three settings are 1.0 × 10<sup>-5</sup> eV/atom, 1.0 × 10<sup>-6</sup> Ha and 4 × 4 × 2, respectively. Besides the plane wave energy cutoff is set to be 667 eV. NG was constructed as a big two-dimensional quasi-rhomboid molecular C<sub>71</sub>H<sub>24</sub>N. The geometry optimizations of the NG, the molecular adsorbates and their composite were done in the Dmol<sup>3</sup> module using a medium quality setting first and then a fine quality setting (the energy displacement tolerance of 1.0 × 10<sup>-5</sup> Ha, the SCF tolerance of

$1.0 \times 10^{-6}$  Ha, the SCF k-mesh of  $1 \times 1 \times 1$ ). During all the geometry optimizations, the Perdew-Burke-Ernzerh (PBE) generalized gradient approximation (GGA) functional has been employed with the empirical dispersion correction method developed by Grimme (DFT-D<sup>3</sup>)<sup>[8]</sup>, which have been proven reliable for describing the long-range van der Waals (vdW) interaction. After the surfaces and structures were fully relaxed, the meta-GGA method with M06-L<sup>[9]</sup> has been employed to calculate the single-point energies. The adsorption energies ( $E_b$ ) were calculated by the equation:

$$E_b = E(\text{adsorbent}) + E(\text{adsorbate}) - E(\text{adsorbent-adsorbate}).$$

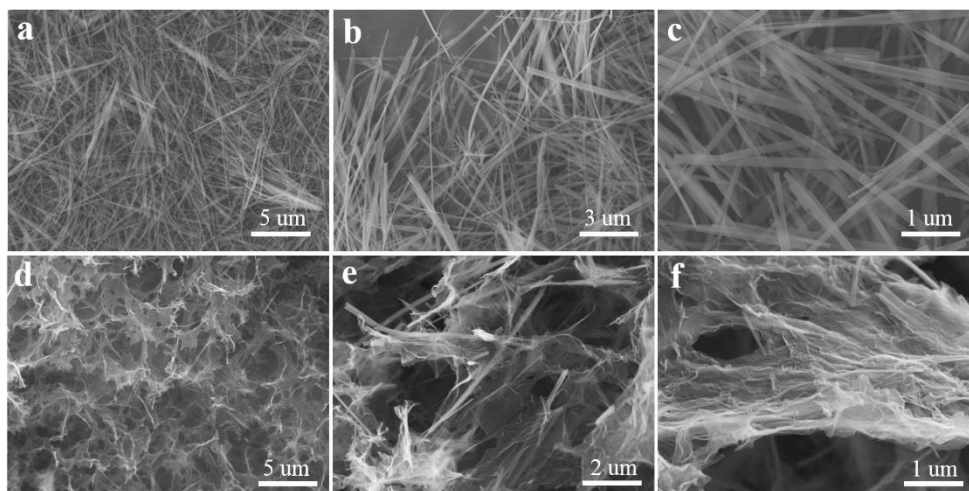


Figure S1. Morphology and structural characterization of the precursor  $\text{H}_2\text{Ti}_3\text{O}_7$  NWs and 3DG/ $\text{H}_2\text{Ti}_3\text{O}_7$ . (a-c) SEM images of  $\text{H}_2\text{Ti}_3\text{O}_7$  NWs and (d-f) SEM images of 3DG/ $\text{H}_2\text{Ti}_3\text{O}_7$ .

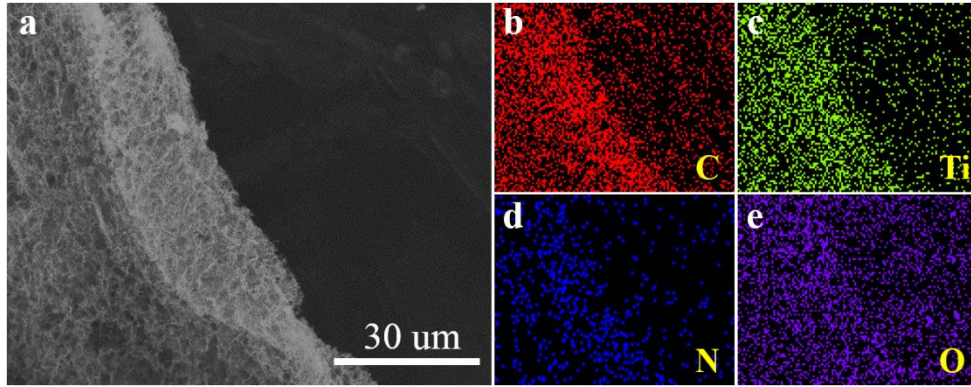


Figure S2. (a) SEM images and (b-e) corresponding elemental mapping images of the 3DNG/TiN.

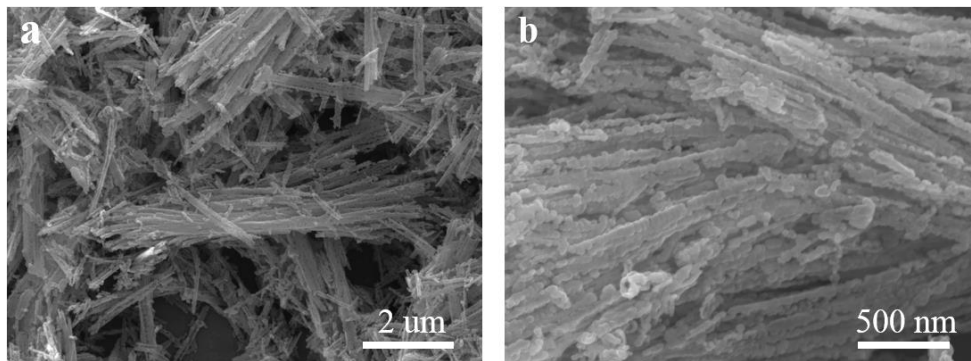


Figure S3. SEM images of the TiN (Derived by annealing  $H_2Ti_3O_7$  nanowires in the same conditions as 3DNG/TiN).

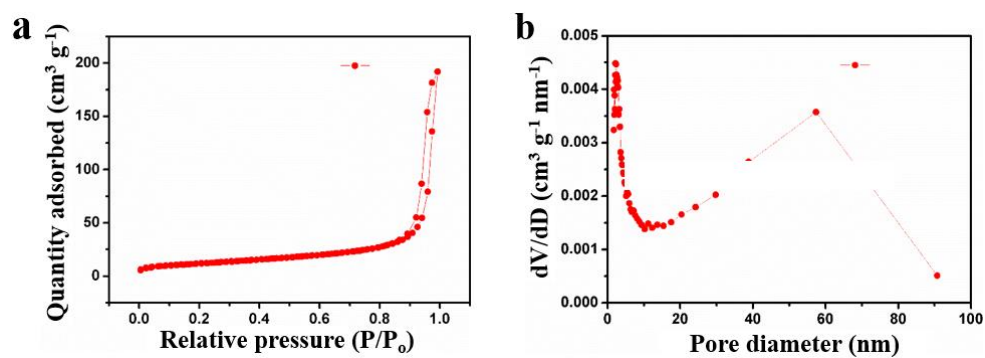


Figure S4. The nitrogen adsorption-desorption isotherm (a) and the pore size distribution curve (b) of TiN.

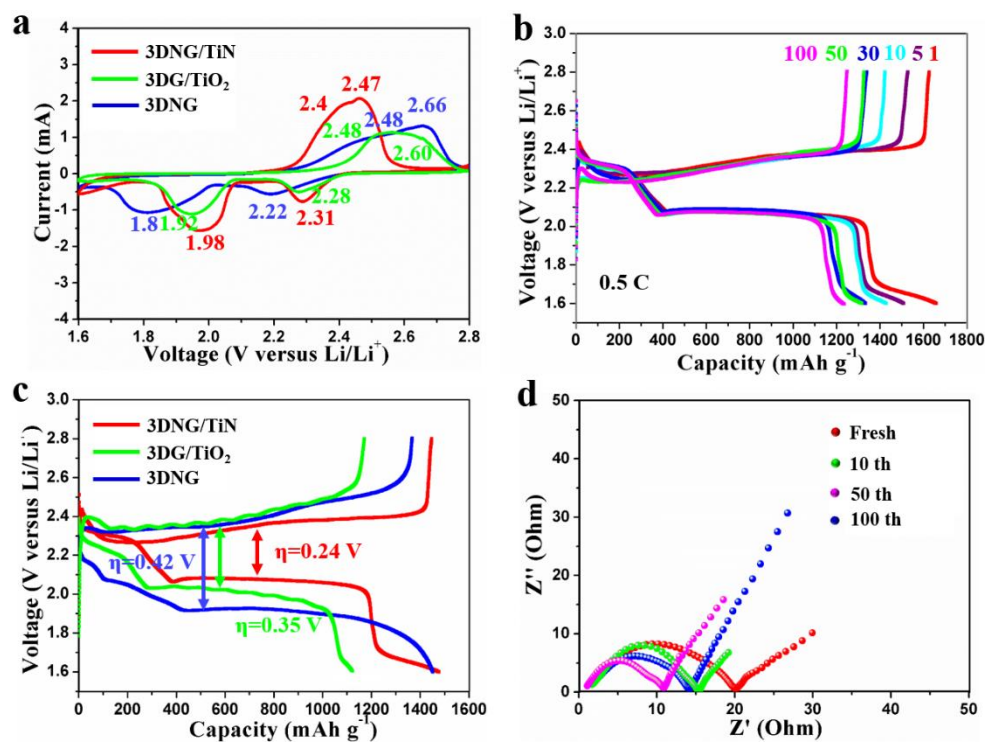


Figure S5. Electrochemical performances of 3DNG/TiN, 3DG/TiO<sub>2</sub> and 3DNG cathodes. (a) The first CV profiles of 3DNG/TiN, 3DG/TiO<sub>2</sub> and 3DNG cathodes at a scan rate of 0.1 mV s<sup>-1</sup>, (b) Galvanostatic charge-discharge profiles of the 3DNG/TiN at 0.5C rate in a potential window from 1.6 to 2.8 V, (c) The first charge-discharge profiles of 3DNG/TiN, 3DG/TiO<sub>2</sub> and 3DNG cathodes at a 0.5C rate, (d) Nyquist plots of 3DNG/TiN cathode at different cycles.

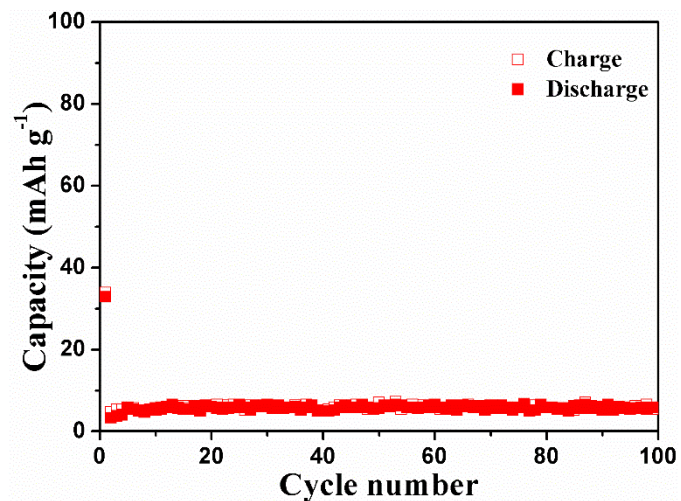


Figure S6. Cycling performance of the 3DNG/TiN composite without  $\text{Li}_2\text{S}_6$  catholyte at the current density of 0.5 C in the voltage range 1.6-2.8 V.

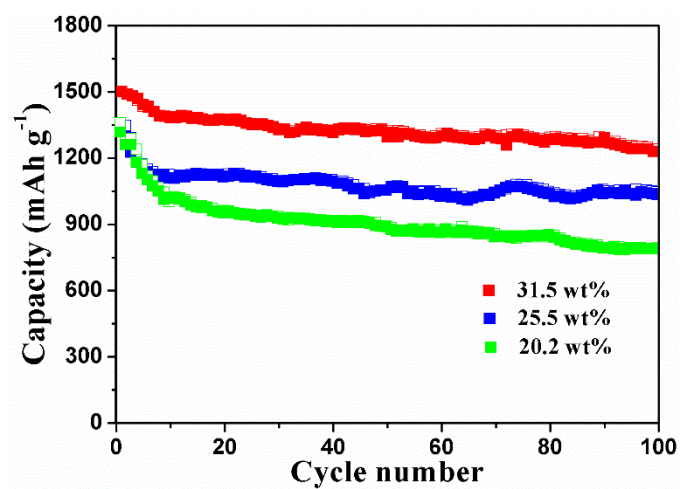


Figure S7. The cycling performance at 0.5 C rate of the 3DNG/TiN with different TiN contents of 31.5%, 25.5%, and 20.2%.

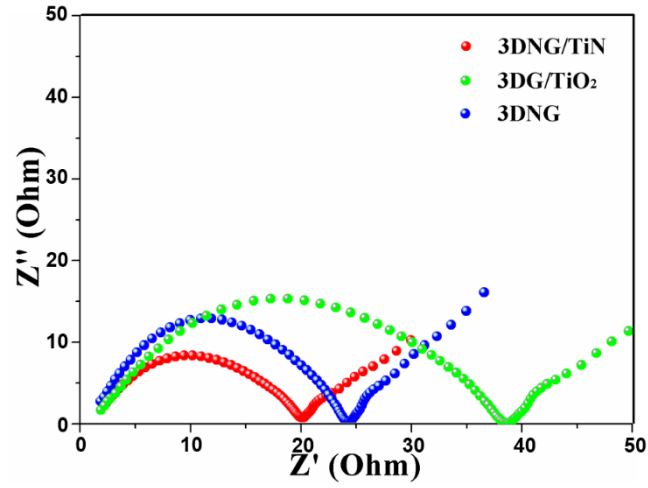


Figure S8. Comparison of the electrochemical impedance spectra of the 3DNG/TiN, 3DNG/TiO<sub>2</sub> and 3DNG cathodes before cycling.

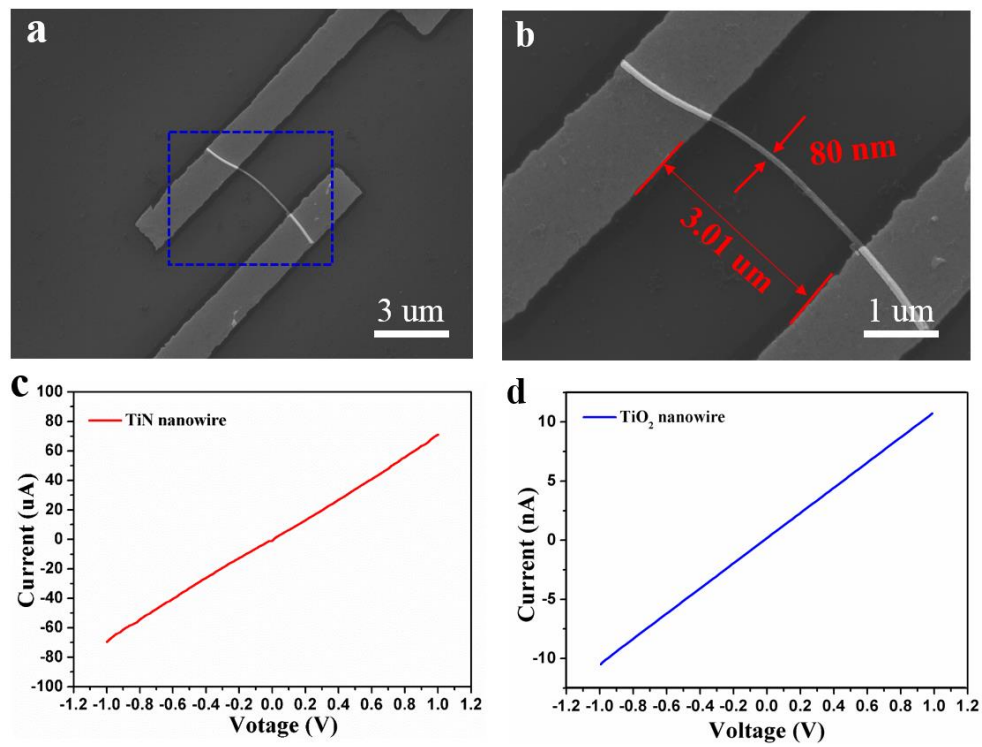


Figure S9. (a, b) SEM images of single TiN nanowire device. The diameter and length of the pristine nanowire correspond to 80 nm and 3.01 μm, respectively. (c, d) I-V curves of TiN and TiO<sub>2</sub> nanowire.

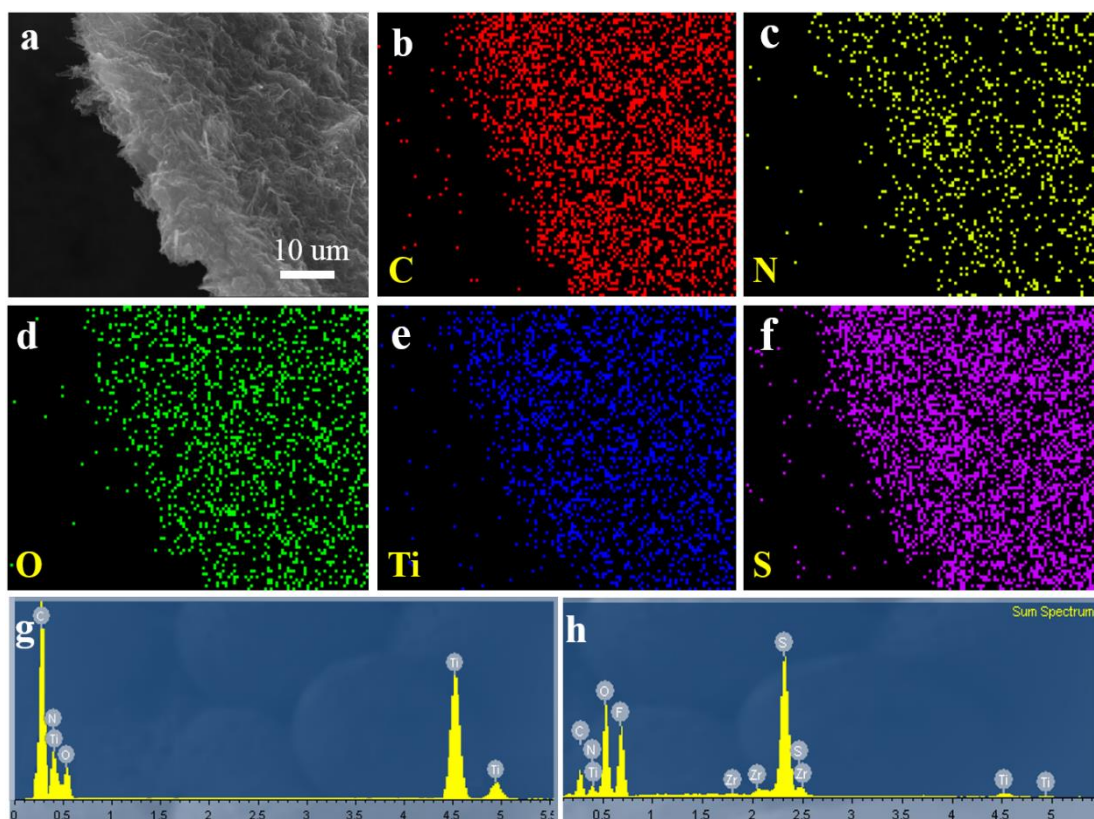


Figure S10. Characterization of cycled 3DNG/TiN at 0.5C for 100 cycles. (a-f) SEM element mappings, (g, h) EDS of 3DNG/TiN before and after cycled, respectively.

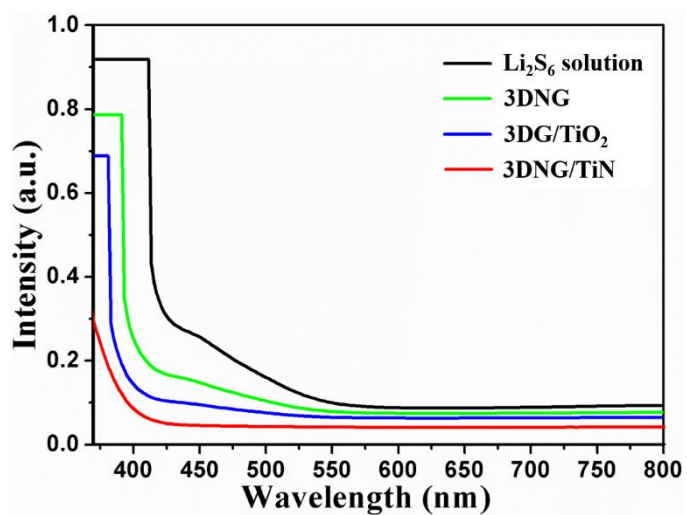


Figure S11. Ultraviolet/visible absorption spectra of Li<sub>2</sub>S<sub>6</sub> solution before and after the addition of 3DNG, 3DNG/TiO<sub>2</sub> and 3DNG/TiN.

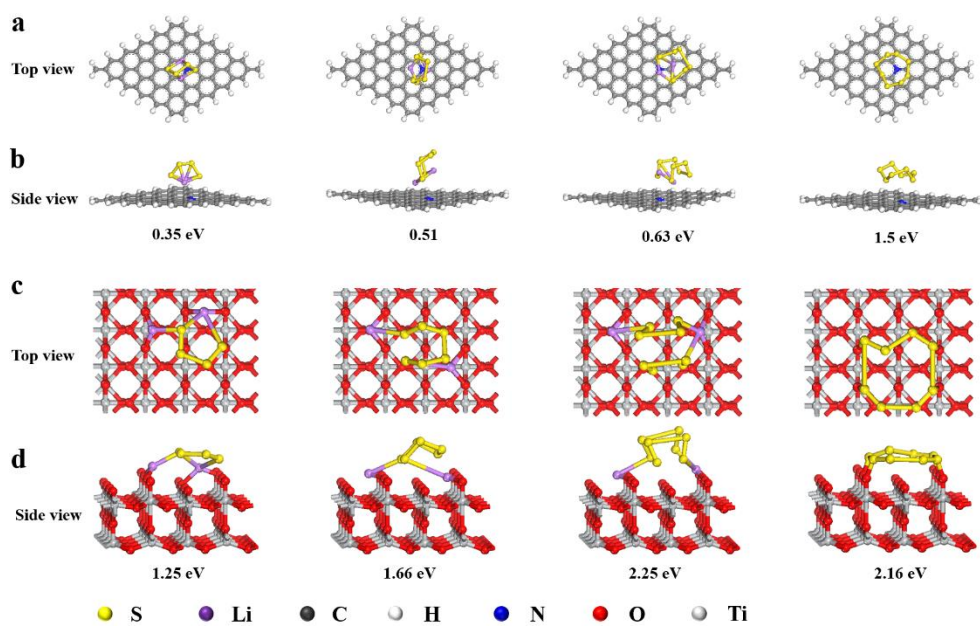


Figure S12. Optimized configurations of the binding of  $\text{Li}_2\text{S}_n$  and  $\text{S}_8$  to the NG and  $\text{TiO}_2$  (110).

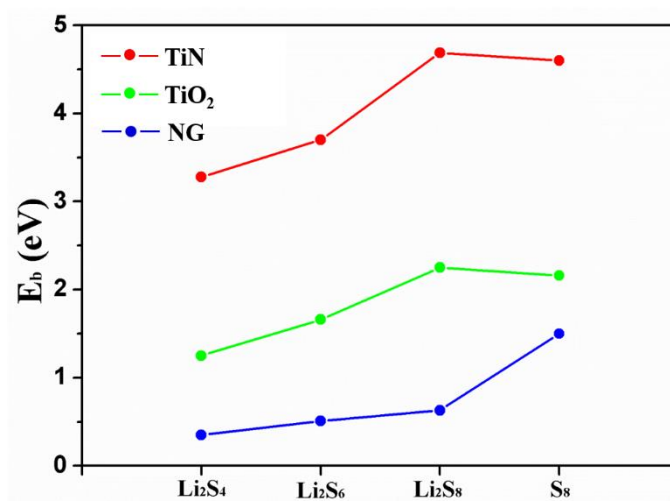


Figure S13. Binding energies for  $\text{LiPSs}/\text{Li}_2\text{S}_n$  on NG,  $\text{TiO}_2$  (110) and TiN (200).

Table S1. Electrochemical performance comparison of various TMNs-based cathodes in Li-S battery

Materials	Mass Loading (mg cm <sup>-2</sup> )	Rate (1C = 1675 mA g <sup>-1</sup> )	Capacity (mAh g <sup>-1</sup> )	Areal capacity (mAh cm <sup>-2</sup> )	Ref.
<b>3DNG/TiN</b>	<b>4.8</b>	<b>0.5 C</b>	<b>1265 (100 cycles)</b>	<b>7.2 (Initial)</b>	<b>This Work</b>
		<b>1 C</b>	<b>957 (200 cycles)</b>		
		<b>5 C</b>	<b>676 (Rate capacity)</b>		
		<b>8.03 mA cm<sup>-2</sup></b>	<b>1255</b>		
	<b>9.6</b>			<b>12.0 (Initial)</b>	
				<b>9.96 (60 cycles)</b>	
TiN-S	1.0	0.5 C 1 C	644 (500 cycles) 776 (Rate capacity)	N/A	28
S/TiN	1.5	0.5 C 5 C	660 (200 cycles) 555 (Rate capacity)	N/A	30
S/TiN-C	1.2	0.5 C 5 C	800 (50 cycles) 700 (Rate capacity)	N/A	29
TiN-S	1.5	0.5 C 1 C	652 (300 cycles) 505.5 (300 cycles)	N/A	25
	4.6	0.77 mA cm <sup>-2</sup>	N/A	3.15 (50 cycles)	
TiN/S	8.7	0.1C	1338 (180 cycles)	N/A	33
7TiN:3TiO <sub>2</sub> -G	1.0-1.2	0.3 C	927 (300 cycles)	N/A	19
	4.3	1 C	331 (2000 cycles)		
TiN/Li <sub>2</sub> S <sub>8</sub>	7	0.1 C	1040 (100 cycles)	N/A	31
VN/G	3.0	0.2 C	1260 (100 cycles)	N/A	27
		1 C	917 (200 cycles)		
		3 C	701 (Rate capacity)		
S-VN/CA	1.3-1.6	0.2 C	1001 (100 cycles)	N/A	26
		1 C	802 (100 cycles)		
S/CNG-10	1.1	0.06 C	505 (600 cycles)	N/A	32
Co <sub>4</sub> N@S	1.5-2.0	0.5 C	1100 (100 cycles)	N/A	24
		1 C	1000 (100 cycles)		
		5 C	494 (1000 cycles)		

Table S2. Comparison of areal capacity of the 3DNG/TiN with that of recent publications in Li-S batteries which have high sulfur loadings more than 4 mg cm<sup>-2</sup>

Mass Loading (mg cm <sup>-2</sup> )	Rate (mA cm <sup>-2</sup> )	Areal capacity (mAh cm <sup>-2</sup> )	Ref.
<b>9.6</b>	<b>8.03</b>	<b>12.0 (Initial) 9.96 (60)</b>	<b>This work</b>
12	2.01	11.5 (Initial) 9.0 (50)	42
5.0	1.68	5.1 (Initial) 4.0 (50)	43
10.5	3.52	8.7 (Initial) 6.7 (100)	44
4.2	0.35 2.0	4.8 (Initial) 2.44 (60)	45
10.2	1.0	10.8 (Initial) 6.0 (50)	46
5.4	4.52	5.43 (Initial) 4.3 (200)	47
6.3	0.53 1.06	6.2 (Initial) 5.0 (60)	48
4.5	1.5	4.3 (Initial) 2.5 (150)	49
7.5	0.63	7.75(Initial)	50
8.1	3.4	7.69 (Initial) 6.8 (50)	51
5.0	0.84 1.68	7.4 (Initial) 6.0 (200)	52
4.7	0.39 1.57	5.8 (Initial) 3.76 (90)	53

[1] R. Armstrong, G. Armstrong, J. Canales, P. G. Bruce, *Angew. Chem. Int. Ed.* **2004**, 43, 2286.

[2] W. S. Hummers, R. E. Offeman, *J. Am. Chem. Soc.* **1958**, 80, 1339.

[3] Y. X. Xu, K. X. Sheng, C. Li, G. Q. Shi, *ACS Nano*, **2010**, 4, 4324.

[4] M. Wang, X. D. Duan, Y. X. Xu, X. F. Duan, *ACS Nano*, **2016**, 10, 7231.

- [5] B. Delley, *J. Chem. Phys.* **2000**, 113, 7756.
- [6] B. Delley, *J. Chem. Phys.* **1990**, 92, 508.
- [7] S. J. Clark, M. D. Segall, C. J. Pickard, P. J. Hasnip, M. I. J. Probert, K. Refson and M. C. Payne, *Z. kristallogr.* **2005**, 220, 567.
- [8] S. Grimme, J. Antony, S. Ehrlich and H. Krieg, *J. Chem. Phys.* **2010**, 132, 154104.
- [9] Y. Zhao, D. G. Truhlar, *J. Chem. Phys.* **2006**, 125, 194101.